ACS APPLIED MATERIALS & INTERFACES

Article

Spectrum-Dependent Spiro-OMeTAD Oxidization Mechanism in Perovskite Solar Cells

Shen Wang, Wen Yuan, and Ying Shirley Meng

ACS Appl. Mater. Interfaces, **Just Accepted Manuscript** • DOI: 10.1021/acsami.5b07703 • Publication Date (Web): 21 Oct 2015

ACS Publications

ACS Applied Materials & Interfaces is published by the American Chemical Society.
1155 Sixteenth Street N.W., Washington, DC 20036

Spectrum-Dependent Spiro-OMeTAD Oxidization Mechanism in Perovskite Solar Cells

Shen Wang, [†] *Wen Yuan,* [‡] *Ying Shirley Meng* [†*]

[†] Department of NanoEngineering, University of California San Diego, 9500 Gilman Drive, La Jolla, CA 92093, USA

[‡] Department of Chemistry, Michigan State University, East Lansing, 48824, USA

KEYWORDS: charge recombination, perovskite solar cells, solid state, p-doping, spectrum, impedance spectroscopy

ABSTRACT

We propose a spectrum-dependent mechanism for the oxidation of 2,2′,7,7′-tetrakis(N,N-di-p-methoxyphenylamine)-9,9′-spirobifluorene (Spiro-OMeTAD) with Bis(trifluoromethane)sulfonimide lithium salt (LiTFSI), which is commonly used in perovskite solar cells as the hole transport layer. The perovskite layer plays different roles in the Spiro-OMeTAD oxidization for various spectral ranges. The effect of oxidized Spiro-OMeTAD on the solar cell performance was observed and characterized. With the initial long wavelength illumination （>450 nm）, the charge recombination at the TiO_2/Spiro-OMeTAD interface was increased due to the higher amount of the oxidized Spiro-OMeTAD. On the other hand, the increased conductivity of the Spiro-OMeTAD layer and enhanced charge transfer at the Au/Spiro-OMeTAD interface facilitated the solar cell performance.

1. Introduction

Hybrid organic-inorganic perovskite solar cells (PSCs) have gained increasing attention as intriguing candidates for next-generation photovoltaic devices since 2010[1]. Recently, 20.1% power conversion efficiency has been achieved through intramolecular exchange reaction[2]. In addition to high efficiencies, PSCs are all-solid-state devices with low cost, a tunable band gap, and a scalable fabrication process, indicating its tremendous commercial prospects[3-8]. The key components of PSCs (which contains meso-porous TiO_2) include the blocking layer, metal oxide photoelectrode, perovskite layer, hole-transport material (HTM), and top electrode[9]. When photons excite the electrons from the valence band (VB) to the conduction band (CB) of the perovskite layer, excitons are generated. The excited electrons are injected into the CB of the metal oxide photoelectrode, and the holes are captured by the HTM in this charge separation process. The photogenerated electrons in the metal oxide are collected by a transparent conductive oxide and go to the external circuit. Electrons will recombine with holes at the top electrode to complete the circuit[10]. The photovoltage of the PSC is equal to the difference between the quasi-Fermi level of the metal oxide photoanode and the redox potential of the HTM[11]. The high hole collection efficiency at the perovskite/ HTM interface is one of the key factors needed to achieve better efficiency in PSCs[12].

One of the major developments for PSCs in recent years is the substitution of the liquid electrolyte to the solid-state HTM 2,2′,7,7′-tetrakis(*N*,*N*-di-*p*-methoxyphenylamine)-9,9′-spirobifluorene (Spiro-OMeTAD). This substitution dramatically improves the stability and the efficiency of PSCs[7, 13]. Unlike the liquid-based electrolyte, which can dissolve the perovskite layer, the small organic molecule

Spiro-OMeTAD, shown in Figure 1(a), is nonreactive to perovskite and is less volatile. The matched band gap with perovskite, amorphous nature, good conductivity with dopants, and high melting point for Spiro-OMeTAD make it one of the most adaptable HTMs in PSCs[14-17]. Recent research demonstrates that a >400 nm thickness of Spiro-OMeTAD HTM layer can guarantee a higher open-circuit voltage and hinder the charge recombination at the TiO_2/HTM interface[18].

Surprisingly, the pristine uncharged form of Spiro-OMeTAD has a relatively low hole mobility and low conductivity before adding a *p*-dopant[19]. Additives play a key role in improving the hole conductivity of the Spiro-OMeTAD layer and ultimately increase the efficiency of PSCs. Bis(trifluoromethane)sulfonimide lithium salt (LiTFSI) has been reported as a *p*-dopant to enhance the conductivity and hole mobility of the Spiro-OMeTAD[16, 20-24]. The function of LiTFSI in PSCs is quite similar to that in solid-state dye-sensitized solar cells (ss-DSSCs). Some of the lithium ions can intercalate into TiO_2 to downshift its conduction band, resulting in a higher photocurrent[25-27]. The rest of the lithium ions can react with oxygen and Spiro-OMeTAD to facilitate the generation of oxidized Spiro-OMeTAD. While the large anion $TFSI^-$, as shown in Figure 1(b), can stabilize the oxidized Spiro-OMeTAD as the counter-ion[19-22, 28, 29].

There are two different proposed mechanisms in the literature on the generation of oxidized Spiro-OMeTAD with the assistance of LiTFSI in DSSCs. Ute B. Cappel et al. proposed a three-step mechanism where sensitizers are excited by photons and then the excited electrons are captured by oxygen. The oxidized Spiro-OMeTAD is created by regeneration of oxidized sensitizer. In the reactions, LiTFSI functions either as a catalyst or a stabilizer of the oxidized Spiro-OMeTAD[20]. The mechanism is

written as:

$$Dye+hv \longrightarrow Dye^* \longrightarrow Dye^+ + e^-(TiO_2) \quad (1)$$

$$e^-(TiO_2)+O_2 \longrightarrow O_2^{\cdot -} \quad (2)$$

$$Dye^+ + Spiro \longrightarrow Dye + Spiro^+ \quad (3)$$

Later, Antonio Abate et al. proposed a two-step mechanism: first, equilibrium between Spiro-OMeTAD with oxygen and oxidized Spiro-OMeTAD (Spiro-OMeTAD$^{\cdot +}O_2^{\cdot -}$) exists; the equilibrium is moved forward by adding LiTFSI, because the superoxide radical O_2^- reacts with Li^+ to form Li_2O and Li_2O_2, and finally Spiro-OMeTAD$^{\cdot +}TFSI^-$ is generated[19]. The mechanism is written as:

$$Spiro\text{-}OMeTAD+O_2 \longleftrightarrow Spiro\text{-}OMeTAD^{\cdot +}O_2^{\cdot -} \quad (4)$$

$$Spiro\text{-}OMeTAD^{\cdot +}O_2^{\cdot -}+LiTFSI \longrightarrow Spiro\text{-}OMeTAD^{\cdot +}TFSI^- + Li_xO_y \quad (5)$$

The major difference between these two mechanisms is whether photons and sensitizers participate in the reactions. In the three-step mechanism, photons trigger the following reactions while the oxidized Spiro-OMeTAD is produced from the regeneration of sensitizers. In the two-step mechanism, neither photons nor sensitizers facilitated the formation of oxidized Spiro-OMeTAD. Moreover, initial illuminating treatment, which means to illuminate a solar cell for a while before testing its efficiency, also plays a key role on enhancing solar cell performance. It can be attributed to the Li^+ migration and Spiro-OMeTAD oxidization[22], which supports the photons participating in the generation of the oxidized Spiro-OMeTAD.

Due to the similar device structure between DSSC and PSCs, the above mechanisms can be adapted to PSCs. Only few studies are focusing on the function of LiTFSI in the PSCs up to now. Exploring the relations between these mechanisms and PSCs can help understanding the function of photons, LiTFSI, and perovskite on the formation of oxidized Spiro-OMeTAD. It would allow us to find rational ways to further

improve the efficiency of PSCs.

Herein, we report a systematic study of the origination of oxidized Spiro-OMeTAD in PSCs. With the combination of UV-Vis, a solar simulator equipped with longpass filters, four-point probe conductivity measurement and electrochemical impedance spectroscopy, a spectrum-dependent mechanism is proposed based on the wide absorption range of perovskite. This mechanism that reconciles the difference in previously proposed mechanisms is applicable for various visible spectrum ranges to increase the amount of oxidized Spiro-OMeTAD and finally, improve the efficiency of PSCs.

2. Experimental Methods

2.1 Reagents and Materials

All materials, unless stated otherwise, were purchased from Sigma Aldrich and used as received. Spiro-OMeTAD was purchased from Merck KGaA.

2.2 Synthesis of CH_3NH_3I

CH_3NH_3I was synthesized according to the reported procedure[30]. 14 ml Methylamine (40% in methanol, TCI) and 15 ml hydroiodic acid were mixed at 0℃ and stirred for an hour. The solution was evaporated at 90℃ for an hour to obtain the deep-brown primary product. The product was re-dissolved in ethanol at 70℃, precipitated and washed with diethyl ether several times until the product turned to white color. Finally, the product was dried at 60℃ in a vacuum oven for 24 h.

2.3 Device Fabrication

Perovskite solar cells were fabricated using the sequential deposition method[6]. FTO glasses (Pilkington, TEC-15) were cleaned by an ultrasonic bath with detergent water, alkaline ethanol solution, and deionized water, sequentially; each cleaning step lasted for 15 min. Then, the oxygen plasma cleaning step was applied for 10 min to remove the last traces of organic residues on the slides.

The TiO_2 blocking layer (BL) was spin-coated on the FTO substrates at 800 r.p.m. for one minute using 0.24 M titanium isopropoxide in 5 ml ethanol solution. The films were annealed at 500℃ for 30 min. After cooling down to room temperature, the films were immersed in 0.03 M aqueous $TiCl_4$ solution at 70℃ for 40 min and then gradually heated at 500℃ for 40 min after washing with deionized water. Commercial TiO_2 paste (Dyesol 18NRT, Dyesol) diluted in ethanol (2:7, weight ratio) was spin-coated on the films at 5,000 r.p.m for 30 sec and the film was annealed at 450℃ for 40 min to form the mesoporous TiO_2 layer.

PbI_2 solution (1 M) was prepared by 462 mg PbI_2 dissolved in 1 mL *N,N*-dimethylformamide (DMF) stirring at 80℃. The solution was spin coated on the films at 5000 r.p.m. for 90 sec. After spinning, the films were dried at 80℃ for 30 min and dipped in 2-propanol for 2 sec. Then the pre-wetted films were dipped in a solution of CH_3NH_3I in 2-propanol (10 mg ml^{-1}) for 2 min and dried at 80℃ for 30 min.

The 2,2',7,7'-teterakis(*N,N*-di-*p*-methoxyphenylamine)-9,9-spirobifluorene (Spiro-OMeTAD) solution was prepared by 100 mg of Spiro-OMeTAD, 28.8 μl 4-*tert*-butyl pyridine (tBP) and 17.7 μl lithium bis(trifluoromethanesulfonyl)imide (LiTFSI) solution (520 mg LiTFSI in 1 ml acetonitrile) in 1 ml of chlorobenzene. The solution was spin-coated on the $CH_3NH_3PbI_3$ layers at 3,000 r.p.m. for 1 min. Finally, 80 nm

of gold was e-beam evaporated on the Spiro-OMeTAD-coated film.

The full perovskite solar cell structure is displayed in Figure 1(c). The image was taken by the bright field transmission electron microscope (BF-TEM). The sample was thinned within 100 nm by focusing ion beam before taking the TEM image.

Devices for measuring the resistance of the hole conductor were fabricated as follows with the Spiro-OMeTAD solution identical to that used for the PSC fabrication, the solution spin-coated on glass substrates with/without perovskite $CH_3NH_3PbI_3$ layer (the perovskite $CH_3NH_3PbI_3$ layer was prepared as the same procedure as the PSC) at 3,000 r.p.m. for 1 min, the Spiro-OMeTAD coated films covered with a 100 μm width spacer, and finally 80 nm of gold e-beam evaporated on the sample.

2.4 Device Characterization

Photocurrent density and voltage (J-V) were measured with a solar simulator with a 150 W xenon lamp (Solar Light SL07265, equipped with an AM1.5G filter, calibrated with a standard Si solar cell to simulate AM1.5 illumination (100 mW cm^{-2})) and a Keithley 2400 source meter. Before the J-V test, the solar simulator was marked with a 450 nm longpass filter to illuminate the perovskite solar cell for one hour and test its efficiency at 0 min, 10 min, 30 min, and 1 h.

Electrochemical Impedance Spectra (EIS) were conducted using a Solartron 1287 electrochemical interface coupled with a Solartron 1455A frequency response analyzer. A 10 mV perturbation was applied, and the frequency was from 1 MHz to 1 Hz. The solar cell was illuminated by the solar simulator which was integrated with the 450 nm longpass filter for 1 h, and the solar cell was tested by the EIS at 0 min, 10 min, 30 min, and 1 h, respectively. Final results for EIS were fit with Z-View (The

equivalent circuit of EIS fitting is shown in Figure S1, Supporting Information. The fitting results are shown in Table S1 in Supporting Information).

Resistance of the hole conductor was tested by four-point probe (Jandel Four-Point Probe with RM3000 Test Unit) measurement with the devices mentioned before in dark condition. The curves on the devices, which were created by the 100 μm spacer, were set between the second and third probe during the test. Before testing, the devices were illuminated on solar simulator with full light, 380 nm longpass filter and 450 nm longpass filter for 0 min, 10 min, 20 min, 30 min, 40 min and 1 h, respectively.

2.5 UV-Vis Spectroscopy

UV−Vis spectra were carried out in an absorption mode on a Lambda 1050 UV−Vis spectrometer. Measurements of the solutions were taken in a 10 mm quartz cuvette placed in a cuvette holder was integrated within the setup. The concentration of Spiro-OMeTAD for the UV-Vis test was 8 μM in chlorobenzene.

3. Results and Discussion

The first aim of this study is to understand the function of photons on the generation of oxidized Spiro-OMeTAD. According to the literature, the major UV-Vis peak for Spiro-OMeTAD is a sharp peak at 395 nm, while oxidized Spiro-OMeTAD is a sharp peak at 400 nm and an additional broad peak around 500 nm[31]. However, as the signal of Spiro-OMeTAD around 395 nm often shields the oxidized Spiro-OMeTAD 400 nm peak, the broad peak around 500 nm is usually considered as the indicator for the generation of oxidized Spiro-OMeTAD[19, 28].

Figure 2(a) and 2(b) show the influence of illumination time on Spiro-OMeTAD with LiTFSI in ambient condition at AM1.5 illumination (100 mW cm^{-2}). The increasing absorption from 600-800 nm also implies the generation of oxidized Spiro-OMeTAD as well, for the broad peak can extend to 800 nm[28]. This illumination time-dependent signal illustrates that photons are participating in the generation of the oxidized Spiro-OMeTAD in ambient condition.

Figure 2(c) and 2(d) show the effect of the LiTFSI concentration on the generation of oxidized Spiro-OMeTAD with the same illumination time; the samples are exposed to AM1.5 illumination (100 mW cm^{-2}) for 1 h. According to Figure 2(d), even without adding lithium salt, after 1 h of illumination the broad 500 nm peak appears which means that LiTFSI is unnecessary for the generation of oxidized Spiro-OMeTAD. With only O_2 and light, Spiro-OMeTAD oxidation can occur. However, with an increasing amount of LiTFSI, the amount of oxidized Spiro-OMeTAD also increased. This phenomenon indicates that although LiTFSI does not function in the generation of oxidized Spiro-OMeTAD, it can facilitate the Spiro-OMeTAD oxidation reaction to move forward. Therefore, LiTFSI acts as a 'secondary reactant' to move forward the primary Spiro-OMeTAD oxidation reaction.

We then investigated the effect of the incident light wavelength on the oxidation reaction. Two different types of longpass filters are separately equipped to the solar simulator to detect whether the reactions are spectrum-dependent. The function of the longpass filter is to control the spectral range. It only allows the photons which have longer wavelength to pass through and illuminate on sample. For instance, the 380 nm longpass filter only allows the light with wavelength longer than 380 nm to pass.

The Spiro-OMeTAD samples, as previously tested, are kept in ambient dark condition for 30 min as the reference sample. According to Figure 3, no peak appears around 500 nm after 30 min when the sample was kept in ambient dark condition. This supports our conclusion that Spiro-OMeTAD oxidization is optically activated.

As mentioned previously, the major absorption peak for Spiro-OMeTAD in UV-Vis spectrum is 395 nm, so it is possible that lower-wavelength light can trigger the following Spiro-OMeTAD oxidization. In contrast, at wavelength longer than 450 nm, no absorption peak appears. The photons in this range (>450 nm) may not be energetic enough to overcome the activation energy for the oxidization reaction. Meanwhile, perovskite has a wide absorption range; the absorption spectrum for $CH_3NH_3PbI_3$ extends to 800 nm while $CH_3NH_3Sn_{0.5}Pb_{0.5}I_3$ extends up to 1050 nm[32]. The wide absorption range indicates that in a long wavelength range (> 450 nm), it is possible that Spiro-OMeTAD oxidization reaction can proceed with the assistance of perovskite. Based on these assumptions, the solar simulator was equipped with 380 nm and 450 nm longpass filters to investigate the spectrum-dependent roles of perovskite in the Spiro-OMeTAD oxidization.

As shown in Figure 3(a) and 3(b), when the wavelength is longer than 380 nm, after 30 min of illumination treatment, the oxidized Spiro-OMeTAD peak will appear regardless of the presence of a perovskite layer. This shows that in this spectrum range, it is unnecessary for perovskite to participate in the Spiro-OMeTAD oxidization. When using the 450 nm longpass filter to illuminate the sample for 30 min, as shown in Figure 3(c) and 3(d), the oxidized Spiro-OMeTAD peak (around 500 nm) only appears in the sample which has perovskite. This result proves that in long

wavelength range, the perovskite sensitizer participates in oxidization. As a result, two mechanisms exist in the formation of the oxidized Spiro-OMeTAD: In 380 to 450 nm spectral range, perovskite is unnecessary for Spiro-OMeTAD oxidization. While in >450 nm spectral range, Spiro-OMeTAD needs the assistance of the perovskite to be oxidized.

We used liquid samples for UV-Vis because UV-Vis cannot rule out the spectral disturbance of the perovskite layer in the solid state. To further prove the spectrum-dependent hypothesis in solid state Spiro-OMeTAD, the conductivity of the hole transport layer was characterized by four-point probe measurement.

The device structure for the four-point probe measurements is shown in Figure 4(a) and 4(b). A 100 μm space is set between the second and third probes on each device to ensure the measurement of the hole transport layer conductivity. After the devices were illuminated by the solar simulator equipped with longpass filters for a specific period of time (from 0 min to 60 min), the conductivity was tested by four-point probe in dark condition in case less current flowed through the perovskite layer. If the Spiro-OMeTAD oxidization occurs, the total amount of ions in the hole transport increases, enhancing the conductivity of the devices.

As shown in Figure 4(c), when the perovskite layer exists, the conductivity of all devices increased. The only difference in Figure 4(c) is that the device which was illuminated with the 450 nm longpass filter light has a conductivity that improves slower than the other two. This can be attributed to the low illumination intensity compared to the full spectral illumination. It indicates that with the assistance of a perovskite layer, at a long wavelength range (>450 nm), Spiro-OMeTAD oxidization

occurs. However, in the perovskite-free device, according to Figure 4(d), even after 60 min of illumination, the 450 nm longpass illumination treatment does not change the device conductivity, which means little or no oxidized Spiro-OMeTAD is generated. The results of the conductivity test are in excellent agreement with the UV-Vis characterization: oxidized Spiro-OMeTAD is generated in the short wavelength range without perovskite, while in the long wavelength range, the generation of oxidized Spiro-OMeTAD is only possible with the assistance of the perovskite.

In order to understand the effect of long wavelength illumination on device performance, we fabricated perovskite solar cells and tested the efficiency after >450 nm illumination initial treatment. As we stated before, in long-wavelength range, photons cannot trigger the Spiro-OMeTAD oxidization without perovskite. If perovskite did not participate in the reaction, no J-V curve change should be observed as the exposure time increases. As shown in Figure 5 and Table 1 however, as the illumination time gets longer, the short circuit current density, fill factor, and cell efficiency improve within 30 min from 10% to 11.9%. This can be attributed to the increasing amount of oxidized Spiro-OMeTAD. The oxidized Spiro-OMeTAD is generated after the long wavelength illumination treatment, and with the assistance of perovskite, more photo-induced electrons can be captured by oxidized Spiro-OMeTAD. As a result, the charge recombination of the solar cell rises at the Spiro-OMeTAD/TiO_2 interface. At the same time, the oxidized Spiro-OMeTAD improves the conductivity and mobility of the hole transport layer. The balance of the negative effect (charge recombination) and positive effect (conductivity improvement) increases the solar cell efficiency in the first 30 min.

After 30 minutes of long wavelength initial illumination treatment, the efficiency of the solar cell slightly decreases. This phenomenon might be more attributed to charge recombination caused by the higher concentration of oxidized Spiro-OMeTAD. The short-term stability issues such as the migration/accumulation of LiTFSI in the hole transport layer[21], the moisture sensitivity, or the degradation of the perovskite layer[33] may cause the slightly decrease of the efficiency as well. In general, the oxidized Spiro-OMeTAD will enhance the efficiency in a short term (< 30 minutes), with a minor decrease in the efficiency afterwards. As shown in Figure S2, Supporting Information, all the PSCs we fabricated are displaying the same behavior after >450 nm illumination initial treatment. We also tested the PSCs after full light illumination initial treatment (Figure S3 and Table S2, Supporting Information). Quite similar behavior compared to the >450 nm illumination initial treatment was observed through the solar cell parameters. The only difference is that the full light treatment cell reaches the maximum fill factor and the efficiency within 10 minutes instead of 30 minutes. This phenomena can be attributed to the oxidized Spiro-OMeTAD can generate faster with the full light illumination treatment than with the >450 nm illumination treatment.

To further investigate the long wavelength light illumination influence on the PSC, electrochemical impedance spectroscopy (EIS) is applied to characterize the interfacial charge transfer and charge recombination of PSCs at various long wavelength illumination times.

The equivalent circuit of this model for PSC (Figure S1, Supporting Information) has been reported[34-35]. R_s represents the series resistance, while R_1 and R_2 correspond to

the charge transfer resistance at the Au/Spiro-OMeTAD and Spiro-OMeTAD/TiO_2 interfaces respectively. According to the Nyquist plot of Figure 6(a) and the fitting results (Table S1, Supporting Information), in the first semi-cycle, which corresponds to R_1, R_1 will decrease with increasing illumination time. It is attributed to the increasing amount of the oxidized Spiro-OMeTAD that reduces the resistance at the Au/Spiro-OMeTAD interface. By reducing R_1, the oxidized Spiro-OMeTAD improves on cell performance. Electrons are easier to transfer from the Au to the hole transport layer with more oxidized Spiro-OMeTAD.

On the other hand, as Figure 6 (b) displays, the second semicircle corresponding to R_2 increases with longer illumination time. It is attributed to the higher amount of oxidized Spiro-OMeTAD which leads to more charge recombination at the Spiro-OMeTAD/TiO_2 interface. Some of the photo-generated electrons in the conduction band of TiO_2 can be trapped by the increasing amount of the oxidized Spiro-OMeTAD. The increasing R_2 means that the oxidized Spiro-OMeTAD also negatively affects the cell performance. Since both the positive and negative effects co-exist for the oxidized Spiro-OMeTAD in the interfaces, the solar cell performance might increase in the first 30 min followed by a minor decrease.

According to EIS, after the long wavelength light treatment, the Spiro-OMeTAD oxidization reaction proceeds with the presence of perovskite. With the results shown, we propose a spectrum-dependent mechanism for the generation of oxidized Spiro-OMeTAD. Both the three-step mechanism[20] and the two-step mechanism[19] are applicable at different spectral ranges for the perovskite solar cells. In a short wavelength range (380-450 nm), our proposed mechanism is similar to the two-step

mechanism, and reactions can be written as:

$$\text{Spiro-OMeTAD}+O_2 \xrightarrow[(380\text{-}450\ \text{nm})]{hv} \text{Spiro-OMeTAD}^{\cdot+}O_2^{\cdot-}$$

$$\text{Spiro-OMeTAD}^{+}O_2^{\cdot-}+Li^{+}TFSI^{-} \longrightarrow \text{Spiro-OMeTAD}^{\cdot+}TFSI^{-}+Li_xO_y$$

While in a long wavelength range (> 450 nm), the three-step mechanism is more suitable with perovskite participating in the oxidization. The reaction is described as follows:

$$\text{Perovskite}+O_2 \xrightarrow[(>450\ \text{nm})]{hv} \text{Perovskite}^{+}O_2^{\cdot-}$$

$$\text{Perovskite}^{+}O_2^{\cdot-}+\text{Spiro-OMeTAD} \longrightarrow \text{Perovskite}+\text{Spiro-OMeTAD}^{\cdot+}O_2^{\cdot-}$$

$$\text{Spiro-OMeTAD}^{\cdot+}O_2^{\cdot-}+Li^{+}TFSI^{-} \longrightarrow \text{Spiro-OMeTAD}^{\cdot+}TFSI^{-}+Li_xO_y$$

It is important to point out that we have not ruled out the possibility that both of the mechanisms co-exist in a short wavelength range (380-450 nm), for perovskite is active in this range as well. Future work will focus on whether these mechanisms co-exist in a short wavelength range, and the percentage of Li_2O_2 and/or Li_2O in these reactions will be characterized. Whether or not the presence of the lithium oxide species has any effect on degradation of PSC is of also our interest.

Conclusion

We demonstrated a spectrum-dependent mechanism for the generation of oxidized Spiro-OMeTAD in a perovskite solar cell and observed its influence on the solar cell performance. Photons are participating in the reaction. In a short wavelength range (from 380 to 450 nm), perovskite is unnecessary for the Spiro-OMeTAD oxidization while in a long wavelength range (> 450 nm), the oxidization reaction can only proceed with the assistance of perovskite. The product, oxidized Spiro-OMeTAD, can improve the conductivity of the hole transport layer, and enhance the charge transfer

at the Au/Spiro-OMeTAD interface. However, it also increases charge recombination at the TiO_2/Spiro-OMeTAD interface. As a result, the initial illumination of a perovskite solar cell can enhance the efficiency, however longer illumination times can reduce the efficiency of PSC. A better interfacial engineering method to hinder charge recombination at the TiO_2/Spiro-OMeTAD interface, while allowing increased generation of oxidized Spiro-OMeTAD would ensure better perovskite solar cell performance.

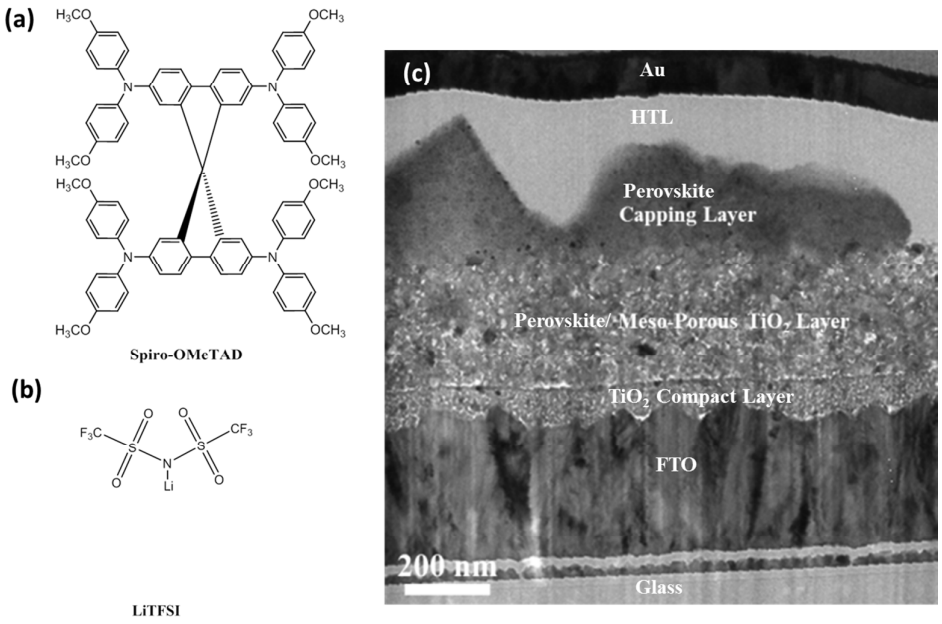

Figure 1. Molecular Structures of (a) Spiro-OMeTAD and (b) LiTFSI; (c) BF-TEM image from cross section view of full Perovskite Solar Cell

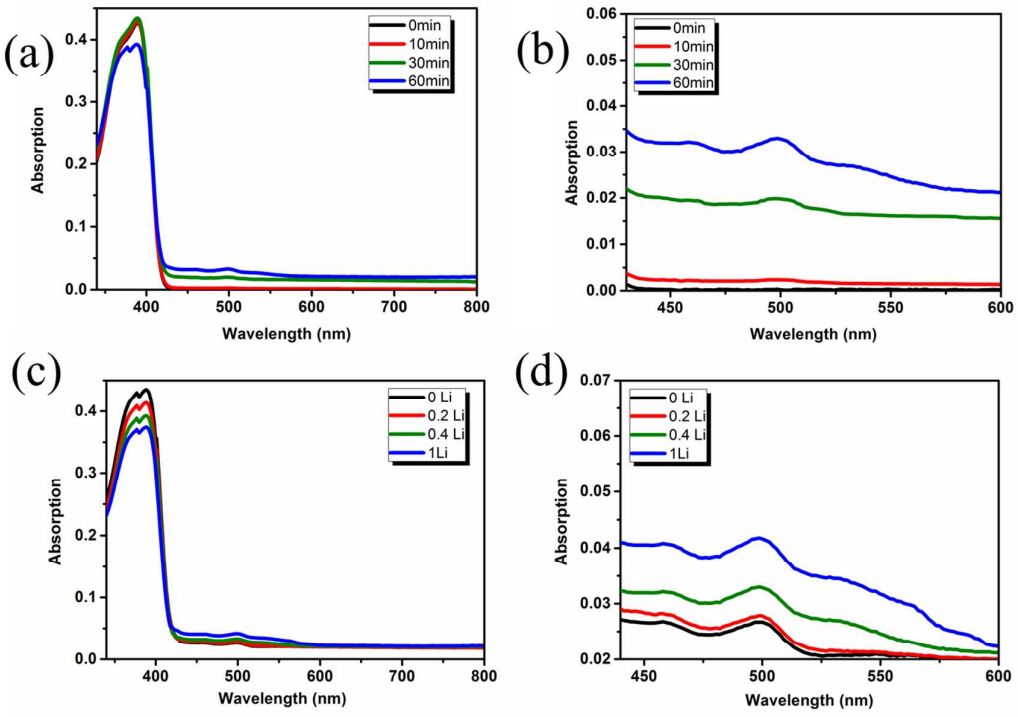

Figure 2. UV-Vis absorption spectra of Spiro-OMeTAD in chlorobenzene at: different illumination time (0 min, 10 min, 30 min and 1 h, respectively) with 0.4 LiTFSI/Spiro-OMeTAD molar ratio (a) is at full spectral range (b) is at 450 nm-600 nm range; and 1 h illumination with different LiTFSI amount (0, 0.2, 0.4 and 1 LiTFSI/Spiro-OMeTAD molar ratio, respectively) (c) is at full spectral range (d) is at 450 nm-600 nm range

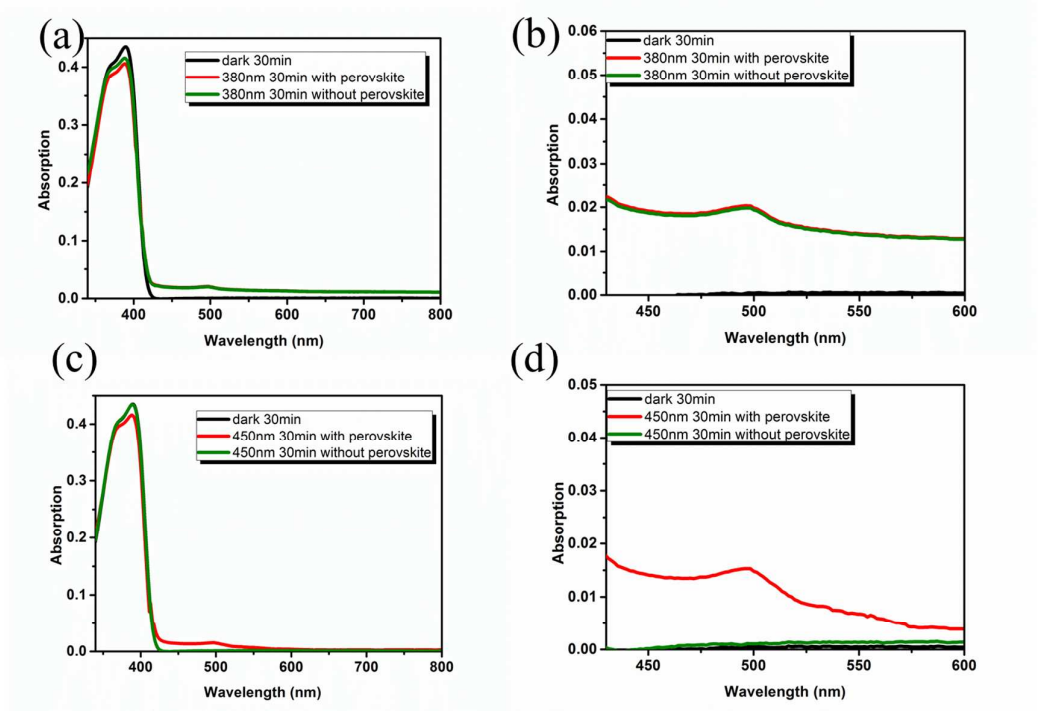

Figure 3. UV-Vis absorption spectra of Spiro-OMeTAD/LiTFSI (0.4 LiTFSI/Spiro-OMeTAD molar ratio) in chlorobenzene with/without perovskite after 30 min illumination by AM1.5 (100 mW cm^{-2}) solar simulator equipped with: 380 nm longpass filter (a) is at full spectral range (b) is at 450 nm-600 nm range; and 450 nm longpass filter (c) is at full spectral range (d) is at 450 nm-600 nm range

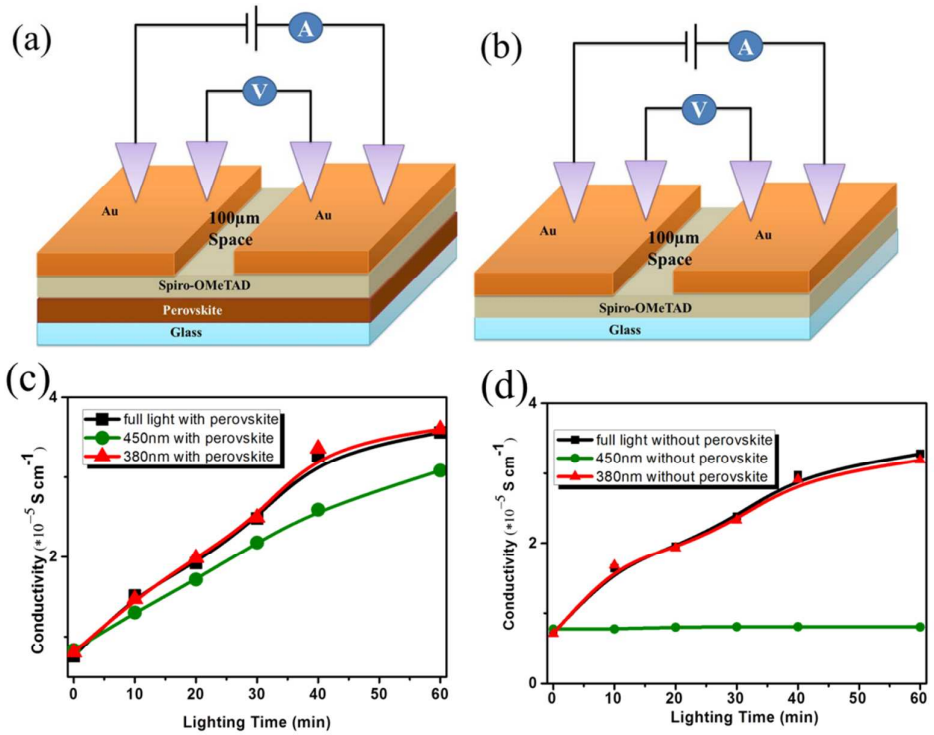

Figure 4. Effective conductivity of the hole transport layer (0.4 LiTFSI/Spiro-OMeTAD molar ratio) at various illumination times and spectral ranges measured by a four-point probe,(a) testing device structure with a perovskite layer, (b) testing device structure without a perovskite layer, (c) effective hole conductivity with perovskite layer, and (d) effective hole conductivity without perovskite layer

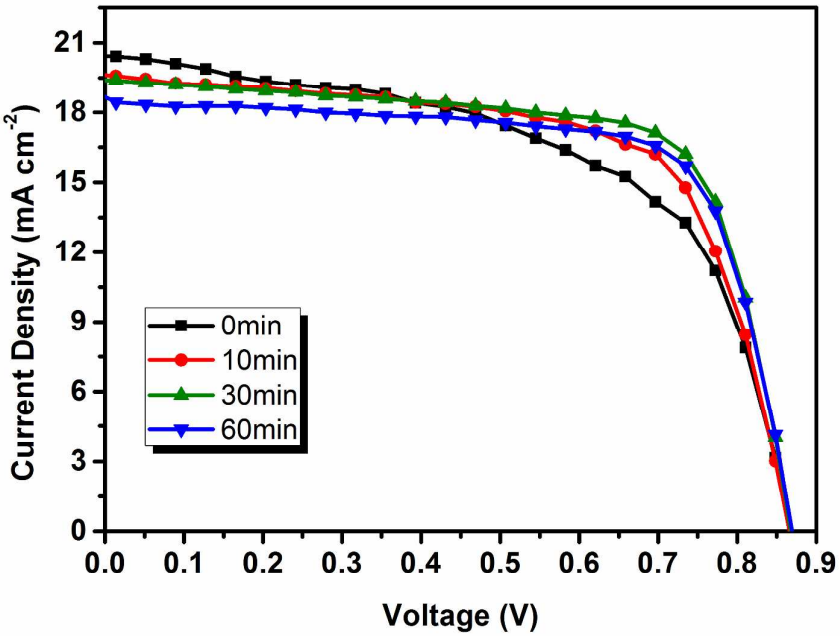

Figure 5. J-V curves of the perovskite solar cells after >450 nm illumination initial treatment

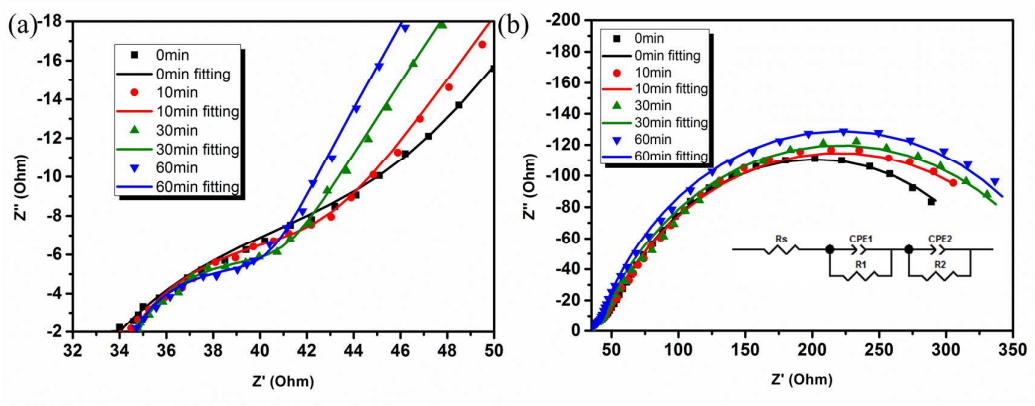

Figure 6. Nyquist plots of the perovskite solar cell with > 450 nm illumination from 0 min to 60 min at a (a) high frequency range and (b) full frequency range. Inset (b) is the equivalent circuit of the PSC

Table 1. Cell parameters of the perovskite solar cells after an initial treatment of > 450 nm illumination

	V_{OC} (V)	J_{SC} (mA/cm^2)	Fill Factor	Efficiency (%)
0min	0.867	20.52	0.56	10.0
10min	0.870	19.68	0.66	11.3
30min	0.862	19.51	0.71	11.9
60min	0.860	18.72	0.71	11.5

Associated Content

Supporting Information

The detailed information on EIS fitting (equivalent circuit and fitting results) is shown in Supporting Information (Figure S1 and Table S1). More J-V curves and cell parameters are displayed in Supporting Information as well (Figure S2, Figure S3 and Table S2). This material is available free of charge via http://pubs.acs.org.

AUTHOR INFORMATION

Corresponding Author

* E-mail (Y.S.M.) shirleymeng@ucsd.edu

Author Contributions

The manuscript was written through contributions of all authors. All authors have given approval to the final version of the manuscript.

Notes

The authors declare no competing financial interest.

Acknowledgements

This work is supported by the seed funding from Sustainable Power and Energy Center (SPEC) under Frontier of Innovation Award by Vice Chancellor of Research at University of California San Diego. S. Wang also gratefully acknowledges the Jacobs Graduate Fellowship by Jacobs School of Engineering at UC San Diego.

Reference

1. Kojima, A.; Teshima, K.; Shirai, Y.; Miyasaka, T. Organometal Halide Perovskites as Visible-Light Sensitizers for Photovoltaic Cells. *J. Am. Chem. Soc.* **2009**, *131*, 6050-6051.

2. Yang, W. S.; Noh, J. H.; Jeon, N. J.; Kim, Y. C.; Ryu, S.; Seo, J.; Seok, S. I. High-Performance Photovoltaic Perovskite Layers Fabricated through Intramolecular Exchange. *Science* **2015**, *348*, 1234-1237.

3. Liu, M.; Johnston, M. B.; Snaith, H. J. Efficient Planar Heterojunction Perovskite Solar Cells by Vapour Deposition. *Nature* **2013**, *501*, 395-398.

4. Zhou, H. P.; Chen, Q.; Li, G.; Luo, S.; Song, T. B.; Duan, H. S.; Hong, Z. R.; You, J. B.; Liu, Y. S.; Yang, Y. Interface Engineering of Highly Efficient Perovskite Solar Cells. *Science* **2014**, *345*, 542-546.

5. Chen, Q.; Zhou, H.; Hong, Z.; Luo, S.; Duan, H. S.; Wang, H. H.; Liu, Y. S.; Li G.; Yang, Y. Planar Heterojunction Perovskite Solar Cells via Vapor-Assisted Solution Process. *J. Am. Chem. Soc.* **2014**, *136*, 622-625.

6. Burschka, J.; Pellet, N.; Moon, S. J.; Humphry-Baker, R.; Gao, P.; Nazeeruddin, M. K.; Grätzel, M.; Sequential Deposition as A Route to High-Performance Perovskite-Sensitized Solar Cells. *Nature* **2013**, *499*, 316-319.

7. Lee, M. M.; Teuscher, J.; Miyasaka, T.; Murakami, T. N.; Snaith, H. J. Efficient Hybrid Solar Cells Based on Meso-Superstructured Organometal Halide Perovskites. *Science* **2012**, *338*, 643-647.

8. Mei, A.; Li, X.; Liu, L.; Ku, Z.; Liu, T.; Rong, Y.; Xu, M.; Hu, M.; Chen, J. Z.; Yang, Y.; Grätzel, M.; Han, H. A Hole-Conductor-Free, Fully Printable Mesoscopic Perovskite Solar Cell with High Stability. *Science* **2014**, *345*, 295-298.

9. Park, N. G. Perovskite Solar Cells: An Emerging Photovoltaic Technology. *Mater. Today* **2015**, *18*, 65-72.

10. Jung, H. S.; Park, N. G. Perovskite Solar Cells: From Materials to Devices. *Small* **2015**, *11*, 10-25.

11. Marchioro, A.; Teuscher, J.; Friedrich, D.; Kunst, M.; van De Krol, R.; Moehl, T.; Grätzel, M.; Moser, J. E. Unravelling the Mechanism of Photoinduced Charge transfer Processes in Lead Iodide Perovskite Solar Cells. *Nat. Photonics* **2014**, *8*, 250-255.

12. Abate, A.; Planells, M.; Hollman, D. J.; Barthi, V.; Chand, S.; Snaith, H. J.; Robertson, N. Hole-Transport Materials with Greatly-Differing Redox Potentials Give Efficient TiO_2-

[CH_3NH_3][PbX_3] Perovskite Solar Cells. *Phys. Chem. Chem. Phys.* **2015**, *17*, 2335-2338.

13. Kim, H. S.; Lee, C. R.; Im, J. H.; Lee, K. B.; Moehl, T.; Marchioro, A.; Moon, S. J.; Humphry-Baker, R.; Yum, J. H.; Moser, J. E.; Grätzel, M.; Park, N. G. Lead Iodide Perovskite Sensitized All-Solid-State Submicron Thin Film Mesoscopic Solar Cell with Efficiency Exceeding 9%. *Sci. Rep.* **2012**, *2*, 1-7.

14. Kwon, Y. S.; Lim, J.; Song, I.; Song, I. Y.; Shin, W. S.; Moon, S. J.; Park, T. Chemical Compatibility Between a Hole Conductor and Organic Dye Enhances the Photovoltaic Performance of Solid-State Dye-Sensitized Solar Cells. *J. Mater. Chem.* **2012**, *22*, 8641-8648.

15. Burschka, J.; Dualeh, A.; Kessler, F.; Baranoff, E.; Cevey-Ha, N. L.; Yi, C.; Nazeeruddin, M. K.; Grätzel, M. Tris(2-(1H-pyrazol-1-yl)pyridine)cobalt(III) as p-Type Dopant for Organic Semiconductors and Its Application in Highly Efficient Solid-State Dye-Sensitized Solar Cells. *J. Am. Chem. Soc.* **2011**, *133*, 18042-18045.

16. Yang, L.; Cappel, U. B.; Unger, E. L.; Karlsson, M.; Karlsson, K. M.; Gabrielsson, E.; Hagfeldt, A.; Johansson, E. M. Comparing Spiro-OMeTAD and P3HT Hole Conductors in Efficient Solid State Dye-Sensitized Solar Cells. *Phys. Chem. Chem. Phys.* **2012**, *14*, 779-789.

17. Leijtens, T.; Ding, I. K.; Giovenzana, T.; Bloking, J. T.; McGehee, M. D.; Sellinger, A. Hole Transport Materials with Low Glass Transition Temperatures and High Solubility for Application in Solid-State Dye-Sensitized Solar Cells. *ACS Nano* **2012**, *6*, 1455-1462.

18. Marinova, N.; Tress, W.; Humphry-Baker, R.; Dar, M. I.; Bojinov, V.; Zakeeruddin, S. M.; Nazeeruddin, M. K.; Grätzel, M. Light Harvesting and Charge Recombination in $CH_3NH_3PbI_3$ Perovskite Solar Cells Studied by Hole Transport Layer Thickness Variation. *ACS Nano* **2015**, *9*, 4200-4209.

19. Abate, A.; Leijtens, T.; Pathak, S.; Teuscher, J.; Avolio, R.; Errico, M. E.; Kirkpatrik, J.; Ball, J. M.; Docampo, P.; McPherson, I.; Snaith, H. J. Lithium Salts as "Redox Active" p-Type Dopants for Organic Semiconductors and Their Impact in Solid-State Dye-Sensitized Solar Cells. *Phys. Chem. Chem. Phys.* **2013**, *15*, 2572-2579.

20. Cappel, U. B.; Daeneke, T.; Bach, U. Oxygen-Induced Doping of Spiro-MeOTAD in Solid-State Dye-Sensitized Solar Cells and Its Impact on Device Performance. *Nano Lett.* **2012**, *12*, 4925-4931.

21. Hawash, Z.; Ono, L. K.; Raga, S. R.; Lee, M. V.; Qi, Y. Air-Exposure Induced Dopant Redistribution and Energy Level Shifts in Spin-Coated Spiro-MeOTAD Films. *Chem. Mater.* **2014**, *27*, 562-569.

22. Yang, L.; Xu, B.; Bi, D.; Tian, H.; Boschloo, G.; Sun, L. ; Hagfeldt, A.; Johansson, E. M.; Initial Light Soaking Treatment Enables Hole Transport Material to Outperform Spiro-OMeTAD in Solid-State Dye-Sensitized Solar Cells. *J. Am. Chem. Soc.* **2013**, *135*, 7378-7385.

23. Kazim, S.; Nazeeruddin, M. K.; Grätzel, M.; Ahmad, S. Perovskite as Light Harvester: A Game Changer in Photovoltaics. *Angew. Chem., Int. Ed.* **2014**, *53*, 2812-2824.

24. Yuan, W.; Zhao, H.; Hu, H.; Wang, S.; Baker, G. L. Synthesis and Characterization of the Hole-Conducting Silica/Polymer Nanocomposites and Application in Solid-State Dye-Sensitized Solar Cell. *ACS Appl. Mater. Interfaces* **2013**, *5*, 4155-4161.

25. Kopidakis, N.; Benkstein, K. D.; van de Lagemaat, J.; Frank, A. J. Transport-Limited Recombination of Photocarriers in Dye-Sensitized Nanocrystalline TiO_2 Solar Cells. *J. Phys. Chem. B* **2003**, *107*, 11307-11315.

26. Yu, Q.; Wang, Y.; Yi, Z.; Zu, N.; Zhang, J.; Zhang, M.; Wang, P. High-Efficiency Dye-Sensitized Solar Cells: The Influence of Lithium Ions on Exciton Dissociation, Charge Recombination, and Surface States. *ACS Nano* **2010**, *4*, 6032-6038.

27. Jennings, J. R.; Wang, Q. Influence of Lithium Ion Concentration on Electron Injection, Transport, and Recombination in Dye-Sensitized Solar Cells. *J. Phys. Chem. C* **2010**, *114*, 1715-1724.

28. Nguyen, W. H.; Bailie, C. D.; Unger, E. L.; McGehee, M. D. Enhancing the Hole-Conductivity of Spiro-OMeTAD without Oxygen or Lithium Salts by Using Spiro(TFSI)(2) in Perovskite and Dye-Sensitized Solar Cells. *J. Am. Chem. Soc.* **2014**, *136*, 10996-11001.

29. Tiwana, P.; Docampo, P.; Johnston, M. B.; Herz, L. M.; Snaith, H. J. The Origin of An Efficiency Improving "Light Soaking" Effect in SnO2 Based Solid-State Dye-Sensitized Solar Cells. *Energy Environ. Sci.* **2012**, *5*, 9566-9573.

30. Im, J. H.; Lee, C. R.; Lee, J. W.; Park, S. W.; Park, N. G. 6.5% Efficient Perovskite Quantum-Dot-Sensitized Solar Cell. *Nanoscale* **2011**, *3*, 4088-4093.

31. Fantacci, S.; De Angelis, F.; Nazeeruddin, M. K.; Grätzel, M. Electronic and Optical Properties

of the Spiro-MeOTAD Hole Conductor in Its Neutral and Oxidized Forms: A DFT/TDDFT Investigation. *J. Phys. Chem. C* **2011**, *115*, 23126-23133.

32. Hao, F.; Stoumpos, C. C.; Chang, R. P.; Kanatzidis, M. G. Anomalous Band Gap Behavior in Mixed Sn and Pb Perovskites Enables Broadening of Absorption Spectrum in Solar Cells. *J. Am. Chem. Soc.* **2014**, *136*, 8094-8099.

33. Guarnera, S.; Abate, A.; Zhang, W.; Foster, J. M.; Richardson, G.; Petrozza, A.; Snaith, H. J. Improving the Long-Term Stability of Perovskite Solar Cells with a Porous Al_2O_3 Buffer Layer. *J. Phys. Chem. Lett.* **2015**, *6*, 432-437.

34. Xiao, Y.; Han, G.; Chang, Y.; Zhang, Y.; Li, Y.; Li, M. Investigation of Perovskite-Sensitized Nanoporous Titanium Dioxide Photoanodes with Different Thicknesses in Perovskite Solar Cells. *J. Power Sources* **2015**, *286*, 118-123.

35. Kim, H. S.; Lee, J. W.; Yantara, N.; Boix, P. P.; Kulkarni, S. A.; Mhaisalkar, S.; Grätzel, M; Park, N. G. High Efficiency Solid-State Sensitized Solar Cell-Based on Submicrometer Rutile TiO_2 Nanorod and $CH_3NH_3PbI_3$ Perovskite Sensitizer. *Nano Lett.* **2013**, *13*, 2412-2417.

Table of Contents Graphic